Xianlin Zheng, Yiqing Lu, Jiangbo Zhao, Yuhai Zhang, Wei Ren, Deming Liu, Jie Lu, James A. Piper, Robert C. Leif, Xiaogang Liu, and Dayong Jin

High-precision pinpointing of luminescent targets in encoder-assisted scanning microscopy allowing high-speed quantitative analysis

Analytical Chemistry, 2016; 88(2):1312-1319

High-precision pinpointing of luminescent targets in encoder-assisted scanning microscopy allows high-speed quantitative analysis

Xianlin Zheng[1], Yiqing Lu[1,*], Jiangbo Zhao[1], Yuhai Zhang[3], Wei Ren[2], Deming Liu[1], Jie Lu[1], Jim A. Piper[1], Robert C. Leif[4], Xiaogang Liu[3,5], and Dayong Jin[1,2]

[1]*Advanced Cytometry Laboratories, ARC Centre of Excellence for Nanoscale BioPhotonics (CNBP), Macquarie University, NSW 2109, Australia*

[2]*Institute for Biomedical Materials and Devices, Faculty of Science, University of Technology Sydney, NSW 2007, Australia*

[3]*Department of Chemistry, National University of Singapore, 3 Science Drive 3, Singapore 117543, Singapore*

[4]*Newport Instruments, 3345 Hopi Place, San Diego, California 92117-3516, USA*

[5]*Institute of Materials Research and Engineering, A*STAR (Agency for Science, Technology and Research), 3 Research Link, Singapore 117602, Singapore*

[*] Corresponding to Y.L. yiqing.lu@mq.edu.au

ABSTRACT

Compared with routine microscopy imaging of a few analytes at a time, rapid scanning through the whole sample area of a microscope slide to locate every single target object offers many advantages in terms of simplicity, speed, throughput, and potential for robust quantitative analysis. Existing techniques that accommodate solid-phase samples incorporating individual micron-sized targets generally rely on digital microscopy and image analysis, with intrinsically low throughput and reliability. Here we report an advanced on-the-fly stage scanning method to achieve high-precision target location across the whole slide. By integrating X- and Y-axis linear encoders to a motorised stage as the virtual "grids" that provide real-time positional references, we demonstrate an Orthogonal Scanning Automated Microscopy (OSAM) technique which can search a coverslip area of 50 × 24 mm^2 in just 5.3 minutes, and locate individual 15-μm lanthanide luminescent microspheres with standard deviations of 1.38 and 1.75 μm in X and Y directions. Alongside implementation of an autofocus unit that compensates the tilt of a slide in the Z-axis in real time, we increase the luminescence detection efficiency by 35% with an improved coefficient of variation. We demonstrate the capability of advanced OSAM for robust quantification of luminescence intensities and lifetimes for a variety of micron-scale luminescent targets, specifically single down-conversion and upconversion microspheres, crystalline microplates, and colour-barcoded microrods, as well as quantitative suspension array assays of biotinylated-DNA functionalized upconversion nanoparticles (UCNPs).

INTRODUCTION

Quantitative luminescence measurements of biomolecules, single cells and tissue specimens in solid phase are particularly valuable for identification and unambiguous confirmation of rare cell types[1-3], time-lapse study of live cells[4-6], profiling of subcellular components and biomolecular expressions[7-9], and a broad range of other diagnostics applications[10-12]. The existing techniques based on digital microscopy[13-16], however, are time-consuming and resource-demanding, as images are typically captured for the entire sample area, or even through three-dimensional space[17-20], followed by stitching and processing to identify and quantitate targets of interest. Their quantification is also less accurate, because different types of noise and background emission interfere in the measurement of absolute intensities, and targets that are randomly located at the periphery of the field-of-view (FOV) have large variation in excitation and detection efficiencies[21-23]. The key to realising a simplified accessible technique for quantitative luminescence measurements lies in the improvements in both the signal-to-background contrast and the pinpointing precision with which each target is brought to the centre of the FOV.

One solution to this problem includes the use of lanthanide luminescent materials exhibiting long lifetimes and/or photon upconversion properties, which are highly useful as either high-contrast molecular probes for direct labelling[24-30] or microsphere-based suspension arrays for high throughput assays[31-33]. Improved sensitivity by orders of magnitude has been demonstrated compared to the conventional fluorescence methods, taking advantage of either time-gated detection or near-infrared (NIR) excitation to remove the autofluorescence background[34-36]. We have also shown recently that luminescence lifetimes of lanthanide-based upconversion materials can be fine-tuned across the microsecond to millisecond range, allowing for creation of temporally multiplexed codes for luminescence detaction[33,37]. In parallel we have developed a controlled synthesis approach for bottom-up production of a library of colour-barcoded heterogeneous micro-rods at low cost[38]. These advances open new opportunities for data storage, document security, and multiplexing assays which allow a large number of labelled biomolecular species to be interrogated simultaneously.

The advantages offered by lanthanide luminescence have further enabled us to develop a novel two-step Orthogonal Scanning Automated Microscopy (OSAM) technique[33,39,40] to quickly locate target analytes in a microscope slide-mounted sample with minimum requirements in data acquisition, storage and processing. Briefly, the initial scan entails continuous sample movement along the X-axis, with a single-element photodetector tube to rapidly identify any randomly-distributed luminescent targets on a slide. By doing this, a sunrise-sunset profile of luminescence signal can be collected when a target passes the microscopy FOV, which gives the X-coordinate for each target. These coordinates guide orthogonal scans along the Y-axis to traverse each target at the centre of the FOV, allowing luminescence intensity and lifetime for each target to be measured at maximum detected signal.

In spite of the advances made in both materials and instrumentation, the precision with which targets can be located within the comparatively large area of a microscope slide has been limited (typically to ±30 μm, large compared with target size) by electronic jitter and mechanical lag of the scanning stage, as well as optical defocusing on the often tilted slide. Truly quantitative luminescence measurement for micron-scale targets lies in interrogation of every individual target under identical illumination and detection conditions with a precision in location which is small compared to the target size. Here we report a major advance in OSAM performance achieved using linear encoders to provide virtual grids of spatial reference in the XY plane, and addition of an autofocus capability which enables us to offset slide tilt in real time. This new Referenced-OSAM (or R-OSAM) achieves order-of-magnitude improvements in the precision of target location and subsequent quantification of luminescence intensity of individual micron-scale targets in real-time during rapid scanning. The performance of the R-OSAM is systematically validated by statistical analysis of luminescent microspheres, microplates and colour-barcoded microrods, as well as suspension array assays of biotinylated-DNA functionalized upconversion nanoparticles (UCNPs).

EXPERIMENTAL SECTION

Optical configuration. Shown in Supporting Figure S1, the R-OSAM is built on an inverted microscope (IX71, Olympus) equipped with a motorised stage (H117, Prior Scientific). Two light sources in addition to the original mercury lamp are integrated: a fibre-coupled near-infrared (NIR) diode laser with peak wavelength at 980 nm (Beijing Viasho Technology; maximum CW laser power 1.3 W), and an ultraviolet light-emitting diode (UV LED) with peak wavelength at 365 nm (NCSU033A, Nichia; bandwidth 9 nm FWHM, maximum CW output 250 mW). A doublet collimator (F810SMA-780, Thorlabs; f = 36 mm) and a fused silica lens (f = 30 mm) are coupled to the additional sources, respectively, to ensure uniformity in illumination. The excitation beam is reflected by a dichroic before illuminating the field-of-view (FOV) through an objective lens (NT38-340, Edmund Optics; 60×, NA = 0.75). The luminescence is directed to either an electronically gateable photomultiplier tube (PMT, H10304-20-NF, Hamamatsu; 10^6 gain at 0.9 V control voltage) or a digital colour camera (DP72, Olympus), switched by a movable mirror placed at 45°. In front of the PMT a convex lens (f = 40 mm) is used to converge the emission onto the photocathode window. Band-pass filters mounted on a filter wheel can be inserted to select target emission bands.

The following dichroic mirrors and filters were used in this work: FF511-Di01 as well as FF750-SDi02 (Semrock) for NIR excitation; 400DCLP (Chroma) for UV excitation; FF01-540/50 and FF01-655/40 (Semrock) for the green and red upconversion emission from Er^{3+}; FF02-475/50 (Semrock) for the blue upconversion emission from Tm^{3+}; 9514-B (New Focus) for the red emission of Eu chelates; and FF01-842/SP-25 (Semrock) for blockage of excitation wavelengths when taking luminescence images.

Linear encoders. Though the position of the motorised stage can be read out on demand, the in-built serial communication does not provide the capability of real-time reading during continuous motion. We therefore added to the X and Y axes of the stage, two miniature linear encoders (MercuryII 1600, MicroE systems) as well as laser tape scales (Supporting Figure S2; the tape scales are attached to the scanning plates, while the encoders are mounted on the immobile frame). Each encoder has a 850 nm infrared laser diode to illuminate the tape scale engraved with 20-μm grating pitches, and a displacement sensor employing ×40 interpolation to deliver two quadrature square-wave outputs with 0.5 μm resolution per count when reading the tape scale that moves with the stage. A computer equipped with a multifunction data acquisition card (PCIe-6363, National Instruments) is used to synchronously record the optical signal from the PMT (transduced by a preamplifier at 10^5 V/A; DLPCA-200, FEMTO) and the displacement output from the encoders, enabling correlation in the form of a luminescence *vs.* position curve.

Autofocus system. To provide the scanning precision along the Z axis (focal length), an autofocus system consisting of a Z-drive and a focus feedback unit (CRISP, Applied Scientific Instrumentation) is integrated into the R-OSAM (Supporting Figure S3). It is designed to compensate the difference in Z positions across the entire sample area, so that individual targets can be interrogated at identical focal length. The Z-drive, incorporating a DC motor and a rotary encoder, is mounted onto the fine focus shaft of the microscope. The focus feedback unit – basically an extra reflective detection module with a LED source (720 nm), a filter cube and a split photodiode – is inserted in the detection path after the original dichroic. The LED is off the optical axis, so that any focus change of the slide results in the lateral displacement of the reflected light, which is detected by the split photodiode (see Supporting Figure S4)[41]. Its signal is conditioned by an in-built log amplifier to provide closed-loop control for the Z-drive. To ensure robust operation, the LED intensity, the log amplifier offset and the photodiode lateral position are carefully adjusted, so that the signal sensitivity in response to focus shift is maximised. In addition, the relative focus height (Z coordinate), monitored by the rotary encoder of the Z-drive, is displayed on the controller of the autofocus system.

Evaluation Samples. Five kinds of lanthanide luminescent samples, as summarised in Table 1, were prepared for comprehensive validation of our new-generation R-OSAM in precise pinpointing of micron-sized targets and quantitative luminescence measurements.

Table 1. Descriptions of the evaluation samples as well as experiments they are used in.

Sample	Description	Use in experiments	Luminescent Image
1	15-µm polystyrene beads incorporating 40-nm $NaYF_4$:Yb,Er UCNPs with 20 mol% Yb^{3+} and 4 mol% Er^{3+}	target pinpointing; focus height analysis; R-OSAM *vs.* image analysis; material characterisation	
2	5-µm polystyrene beads containing Eu complexes (i.e. FireRed™)	quantification enhancement	
3	barcoded upconversion microrods (width 1~1.5 µm) with $NaYb_{0.995}F_4$:$Tm_{0.005}$ in the middle (length ~1 µm) and $NaYb_{0.999}F_4$:$Er_{0.001}$ at the ends (length ~3 µm each side)	material characterisation	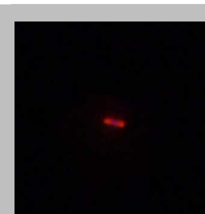
4	upconversion microplates of $NaYb_{0.96}F_4$:$Er_{0.04}$ (size ~4 µm, thickness ~0.5µm)	R-OSAM *vs.* image analysis	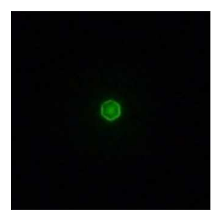
5	streptavidin-modified 15-µm polystyrene beads reacted with biotinylated-DNA functionalised UCNPs	suspension array assays	

Polystyrene microspheres were used as carriers to embed both upconversion and down-conversion luminescent materials via swelling methods. The $NaYF_4$:Yb,Er upconversion nanoparticles (UCNPs; doped with 20% Yb^{3+} and 4% Er^{3+}, size ~40 nm; see Supporting Figure S5 for the Transmission Electron Microscopy image) were synthesized with their oleic acid surfactants removed and incorporated into 15 μm polystyrene beads (PC07N/8783, Bangs Laboratories) according to existing protocols[32,37]. The Eu-complex-containing FireRed™ beads (5 μm in diameter, Newport Instruments) were prepared according to the protocol reported previously[42].

Hydrothermal synthesis was employed for the controlled growth of micron-sized upconversion crystals. The upconversion microrods (middle section $NaYbF_4$:Tm with 99.5% Yb^{3+} and 0.5% Tm^{3+}; end sections $NaYbF_4$:Er with 99.9% Yb^{3+} and 0.1% Er^{3+}; length ~7 μm, width 1~1.5 μm) were synthesized using our reported protocol[38]. A similar method was used to synthesize the microplates ($NaYbF_4$:Er, with 96% Yb^{3+} and 4% Er^{3+}; size ~4 μm, thickness ~0.5μm).

To demonstrate the quantitative suspension array assays, firstly, we functionalised streptavidin (SA) onto the polystyrene beads as the capture substrate (suspension arrays). 50 ul of the 15 μm polystyrene beads were first washed twice by water, and then added into 400 μl MES buffer containing 20 μl of 2.5 mg/ml SA and 5 mg 1-Ethyl-3-(3-dimethylaminopropyl)carbodiimide (EDC). The mixture was incubated at 1,000 rpm for 2 hours. The SA-beads were harvested by centrifugation and washing, and finally stored in 200 μl water. Secondly, the biotinalyted-DNA functionalized UCNPs, as the reporter analytes, were prepared based on a previously reported method[43]. 20 μl of 10 mg/ml UCNPs were suspended in 400 μl chloroform, and then mixed with 300 μl 50 mM 2-(*N*-morpholino)ethanesulfonic acid (MES) buffer containing 6.5 μM biotinylated DNA (Sequence: 5'-GAA ACC CTA TGT ATG CTC TTT TTT TTT T-BIOTIN-3', Integrated DNA Technologies). The mixture was incubated at 600 rpm for 2 hours to perform ligand exchange on the surface of UCNPs from the original oleic acid to the biotinylated DNA.

As a result, the UCNPs were transferred from the chloroform to the MES buffer. The latter was collected and centrifuged at 14,600 rpm for 5 mins. After removing the supernatant containing unbound biotinylated DNA, the functionalized UCNPs were redispersed into 100 μl deionised water. The concentration was 2 mg/ml (corresponding to 15.6 nM)[35] assuming no loss in the preparation steps above. Finally, the assay was conducted by mixing 10 μl of the as-prepared biotinalyted-DNA functionalized UNCPs (10 μl × 15.6 nM = 156 fmol) or its dilution (10, 50 and 200 times) with 5 μl of the SA-beads. The reaction was allowed for 3 hours at room temperature, and the unbound UCNPs were washed away before luminescence measurement.

To prepare the samples for scan, each 20 μl suspension of microspheres, microplates or microrods (~2×10^4 particle/ml after dilution with ethanol) were spread on one coverslip of 50 mm × 24 mm, which was pre-heated to 60 °C to facilitate evaporation of the liquid. The coverslip was then sealed with a microscopic slide. Flip of the sample was avoided to ensure that particles stuck to only one surface. Alternatively, adherent surface treatment or spin coating can be applied.

RESULTS AND DISCUSSION

High-speed scanning by R-OSAM. The concept of the Referenced-OSAM (R-OSAM) employing the linear encoders and the autofocus unit is illustrated in Figure 1a. It rapidly scans sample slides containing luminescent targets by taking advantage of the negligible autofluorescence and scattering background obtained via either time-gated detection or NIR illumination for the upconversion materials, while both the spatial referencing and the autofocusing are carried out in real time without affecting the scan speed. For every slide, its entire area is first examined in a serpentine pattern consisting of continuous movement along one (X) axis and stepwise movement along the other (Y) axis. As shown in Figure 1b, when a target is scanned continuously across the FOV, its luminescence signal exceeds a preselected threshold (V_{th}), so that the entrance (P_1) and exit (P_2) positions are registered. The target coordinate along the scanning direction (X) is calculated out (as $P = (P_1 + P_2)/2$) regardless of variation in the scanning speed. The other coordinate is obtained by a series of orthogonal scans along the Y axis across each target particle, during which the luminescence intensity is captured when the target is exactly at the centre of the FOV. Scanning a coverslip area of 50 × 24 mm^2 typically takes 5.3 minutes, corresponding to an analytical speed of 225 mm^2/minute. R-OSAM can be operated in either the continuous-wave mode or the time-gating mode, as described below.

Precise target pinpointing assisted by encoders. To evaluate the enhanced precision of target location achieved by the linear encoders, the XY coordinates of each targets obtained via orthogonal scanning were sequentially retrieved for image verification with their distance to the centre of the FOV measured. Figure 2a shows data from one typical slide containing 571 UCNP-impregnated beads (15 µm in diameter) pinpointed during rapid scanning under continuous-wave NIR (980 nm) excitation and PMT detection. The standard deviations of the distances from individual beads to the centre of the FOV in X and Y directions were 1.38 and 1.75 µm, respectively, demonstrating that the R-OSAM is capable of target location with precision substantially smaller than the diameter of most targets of practical interest.

To determine the improved precision of R-OSAM in locating down-conversion luminescent targets, the time-gating mode consisting of periodic pulsed UV excitation and delayed detection was employed. With 200 µs time-gating cycles consisting of 90 µs excitation, 10 µs time delay and 100 µs detection window, standard deviations of 4.01 and 3.74 µm were achieved in X and Y directions, respectively, which are about one order of magnitude better than the OSAM scanning result without the assistance of the linear encoders (33.0 and 35.6 µm), as shown in Supporting Figure S6. Because in the time-gating mode a proportion of the targets pass the FOV during the excitation phases when the detector is disabled, location of them is virtually rounded into the adjacent detection phases, leading to slightly decreased precision compared to the continuous-wave mode.

Offsetting Z-axis variance by autofocus. In addition to high-precision XY target location, accurate luminescence measurement also requires bringing all the targets to focus in the Z axis. Figure 2b shows the variance in focus height over a typical slide measured by the autofocus system (with feedback control disabled) upon each target after retrieval as well as the edges of the slide and the coverslip, which displays both the random positions of each targets between the slide and the coverslip and the tilt of slide itself. It is seen that the latter is usually the major cause of the variance in focus height (~70 μm; in contrast the space between the slide and the coverslip is ~20 μm) during the whole slide scanning[44], while the former can be further alleviated with careful sample preparation. By implementing the autofocus system, the focal length is locked with respect to one reflective surface, which essentially compensates the tilt of the sample in real time. The enhanced target location and autofocus of the R-OSAM is demonstrated in Supporting Movie S1.

Improved luminescence quantification by R-OSAM. The precision of R-OSAM in pinpointing the targets in three dimensions further enhances luminescence quantification with maximised excitation and collection efficiencies. As a result, the average intensity measured from single 5-μm Eu-containing FireRed™ beads increased by 35% compared with the OSAM with both the encoders and the autofocus unit disabled, as shown in Figure 2c. Moreover, the recorded intensity histogram shows better symmetry with coefficient of variation (CV) improved from 17.0% to 12.7%.

Comparison of quantitative results obtained by R-OSAM *vs.* image analysis. The intensity captured by the single-element PMT detector during the R-OSAM on-the-fly scanning mode was further validated by analysing the images of each target taken at the retrieval step. Figure 3a shows a good correlation (R-square 0.98 for the linear curve fitting) over a large dynamic range by comparing the two approaches in quantifying the intensities of UCNP-impregnated beads. This consistency extends to the upconversion microplates with size of 4 μm or less (Figure 3b; R-square 0.95 for the linear curve fitting), suggesting that the R-OSAM gives results comparable to the best conventional image analysis while significantly reducing the processing time.

High-throughput material characterization by R-OSAM. Fluorescence microscopy has been conventionally used to assess the quality and dispersity of lanthanide luminescent materials, but the limited number of images by low-throughput image acquisition and analysis are insufficient to give statistical results. We have developed an analytical application of the R-OSAM scanning microscopy method for statistical characterisation of a new type of luminescence materials – the epitaxial-grown barcoded upconversion microrods. Figure 4a shows that the as-prepared crystalline microrods have high-quality consistent core section ($NaYbF_4$:Tm) with a narrow CV in the blue luminescence intensity of only 4.93%, but the high CV in the red luminescence intensity of 39.5% reveals substantial variation in growth of the end sections ($NaYbF_4$:Er). These results were confirmed by target retrieval showing that the individual variation is attributed to the inconsistency during epitaxial growth in terms of different lengths and crystalline quality. In fact, a small but significant proportion of the microrods have single ends (see Figure 4a).

In general, the concentrations of sensitizers (Yb) and activators (Tm or Er) in upconversion materials primarily determine the luminescence lifetimes[37]. To further assess the doping uniformity during the crystal growth, we collected the luminescence lifetimes of each individual barcoded microrods. Figure 4b displays the statistics of the luminescence lifetimes for both the blue (Tm) and the red (Er) emissions, yielding CVs of 6.16% and 3.52% (as well as average value of 366 μs and 444 μs), respectively. This indicates that dopant concentration of end sections has relatively small variation across the population of microrods, thus the large CV for intensity is attributed to variation in the size of the Er-doped end sections.

Moreover, the ratiometric scattering plots by R-OSAM, as shown in Figure 4c, suggest a statistical approach to robust decoding and classification of individual microspheres for multiplexing, in a similar manner to standard flow cytometry assays. Doping UCNPs by 20 mol% Yb and 4 mol% Er yields a consistent green-to-red ratio of 0.526, while doping 99.9 mol% Yb and 0.1 mol% Er yields a consistent green-to-red ratio of 0.0894, with R-square over 0.99 when linear curve fitting is applied. The intrinsic ratios reflect the specific types of the UCNPs used, independent of the exact number of UCNPs embedded in each microsphere.

Quantitative suspension assay assays. Suspension array assays provide a high-throughput analytical approach to screening and quantification of multiple biomolecules in a single test[45,46]. These are based on ensembles of spectrally coded microspheres, most commonly using varying combinations of fluorescent dyes[47-49]. While they have major advantages including rapid reaction kinetics, high throughput and statistical accuracy, their potential for quantitative assays is often compromised, because colour-coded microspheres will also generate spectral-channel interference in the fluorescence detection of the reporter dyes. To remove such interference for accurate quantification, we use lanthanide materials as the reporter probes that can be completely distinguished in the time domain. Such an assay was demonstrated here by using the UCNPs as the reporter probes and the R-OSAM in the time-gating mode for quantitative background-free luminescent measurement. Figure 5a illustrates our experiment by mixing the as-prepared biotinalyted-DNA functionalized UNCPs with the SA-modified polystyrene beads, with different amount of the UCNPs used to evaluate the quantification accuracy. As shown in Figure 5b, the time-gated luminescence signal drops largely linearly as the dilution of the UCNPs, with the intensity CV around 20% for each sample. Similar results can be obtained via retrieval of every target followed by conventional image analysis (see Supporting Figure S7), however this is at the cost of a very long data collection process. This demonstration not only reinforces the practical value of R-OSAM scanning at high speed for precise quantification of target luminescence, but also demonstrates the advantage of using UCNPs as reporter probes to remove the optical background for quantitative suspension array assays.

CONCLUSIONS

By integrating the XY-axes linear encoders and the Z-axis autofocus system into a motorised-stage-based scanning microscopy, precise pinpointing of luminescent targets at an analytical speed of 225 mm^2/minute is realised in this work. Its precision, measured as the distances from the pinpointed targets to the centre of the field of view, is 1.38 and 1.75 μm in X and Y directions respectively, demonstrating that the R-OSAM is capable of target location with precision substantially smaller than typical micron-sized targets. The use of the autofocus system to lock the optical focus to one reflective surface has essentially compensated the tilt of the sample slide in real time. These new advances deliver the best precision in target pinpointing in three dimensions during rapid scanning over a whole microscopic slide, enabling accurate quantification of the luminescence intensities as well as derivative properties such as ratios and lifetimes upon individual targets.

Our R-OSAM approach benefits from the low-background nature of lanthanide luminescence that are immune to the autofluorescence and scattering background via time-gated detection and/or NIR illumination for upconversion materials. It offers a robust and high-throughput solution beyond conventional image analysis for statistical characterisation of luminescence materials. Compared to measurements from collective samples using common spectroscopy and microscopy approaches, the statistical results obtained by R-OSAM provide an array of in-depth information on population variations from one target to another. Such measurement was previously not possible in the routine materials syntheses and characterisations, but will enable new understanding and development of advanced materials for quantitative applications that exploit combinations of colours, intensities, lifetimes and spatial barcodes for high-throughput analysis. Moreover, we demonstrate the upconversion nanoparticles as background-free reporter probes suitable for quantitative biomolecular assays based on the suspension arrays, opening new opportunities in analytical chemistry, micro and molecular biology, pharmaceutical discoveries and clinical diagnostics.

Acknowledgements

This project is financially supported by the Australian Research Council (Linkage Infrastructure, Equipment and Facilities LE150100177, Linkage Project LP140100462, Centre of Excellence for Nanoscale BioPhotonics, and Future Fellowship of D.J. FT130100517), Macquarie University Research Fellowship (Y.L.) and Macquarie University Research Excellence Scholarships. Y.L. acknowledges the ISAC Scholar program of the International Society for Advancement of Cytometry.

Supporting information

Additional information as noted in text. This material is available free of charge via the Internet at http://pubs.acs.org.

Competing financial interests

The authors declare no competing financial interests.

REFERENCES

(1) Chan, L. L.-Y.; Shen, D.; Wilkinson, A. R.; Patton, W.; Lai, N.; Chan, E.; Kuksin, D.; Lin, B.; Qiu, J. *Autophagy* **2012**, *8*, 1371-1382.

(2) Chan, L.-Y.; Cohen, D.; Kuksin, D.; Paradis, B.; Qiu, J. *J Fluoresc* **2014**, *24*, 983-989.

(3) Chen, F.; Lu, J.-r.; Binder, B. J.; Liu, Y.-c.; Hodson, R. E. *Applied and Environmental Microbiology* **2001**, *67*, 539-545.

(4) Krylov, S. N.; Zhang, Z.; Chan, N. W. C.; Arriaga, E.; Palcic, M. M.; Dovichi, N. J. *Cytometry* **1999**, *37*, 14-20.

(5) Han, H.-S.; Niemeyer, E.; Huang, Y.; Kamoun, W. S.; Martin, J. D.; Bhaumik, J.; Chen, Y.; Roberge, S.; Cui, J.; Martin, M. R.; Fukumura, D.; Jain, R. K.; Bawendi, M. G.; Duda, D. G. *Proceedings of the National Academy of Sciences* **2015**, *112*, 1350-1355.

(6) Ball, D. A.; Lux, M. W.; Adames, N. R.; Peccoud, J. *PLoS ONE* **2014**, *9*, e107087.

(7) Erenpreisa, J.; Erenpreiss, J.; Freivalds, T.; Slaidina, M.; Krampe, R.; Butikova, J.; Ivanov, A.; Pjanova, D. *Cytometry Part A* **2003**, *52A*, 19-27.

(8) Fowler, T. L.; Bailey, A. M.; Bednarz, B. P.; Kimple, R. J. *Biotechniques* **2015**, *58*, 37-39.

(9) Hu, S.; Zhang, L.; Krylov, S.; Dovichi, N. J. *Analytical Chemistry* **2003**, *75*, 3495-3501.

(10) Ymeti, A.; Li, X.; Lunter, B.; Breukers, C.; Tibbe, A. G. J.; Terstappen, L. W. M. M.; Greve, J. *Cytometry Part A* **2007**, *71A*, 132-142.

(11) Rossnerova, A.; Spatova, M.; Schunck, C.; Sram, R. J. *Mutagenesis* **2011**, *26*, 169-175.

(12) Ito, H.; Oga, A.; Ikemoto, K.; Furuya, T.; Maeda, N.; Yamamoto, S.; Kawauchi, S.; Itoh, H.; Oka, M.; Sasaki, K. *Cytometry Part A* **2014**, *85*, 809-816.

(13) Galbraith, W.; Wagner, M. C. E.; Chao, J.; Abaza, M.; Ernst, L. A.; Nederlof, M. A.; Hartsock, R. J.; Taylor, D. L.; Waggoner, A. S. *Cytometry* **1991**, *12*, 579-596.

(14) Allalou, A.; Wählby, C. *Computer Methods and Programs in Biomedicine* **2009**, *94*, 58-65.

(15) Szalóki, N.; Doan-Xuan, Q. M.; Szöllősi, J.; Tóth, K.; Vámosi, G.; Bacsó, Z. *Cytometry Part A* **2013**, *83*, 818-829.

(16) Furia, L.; Pelicci, P. G.; Faretta, M. *Cytometry Part A* **2013**, *83A*, 333-343.

(17) Rigaut, J. P.; Vassy, J.; Herlin, P.; Duigou, F.; Masson, E.; Briane, D.; Foucrier, J.; Carvajal-Gonzalez, S.; Downs, A. M.; Mandard, A.-M. *Cytometry* **1991**, *12*, 511-524.

(18) Beliën, J. A. M.; van Ginkel, H. A. H. M.; Tekola, P.; Ploeger, L. S.; Poulin, N. M.; Baak, J. P. A.; van Diest, P. J. *Cytometry* **2002**, *49*, 12-21.

(19) Ragan, T.; Sylvan, J. D.; Kim, K. H.; Huang, H.; Bahlmann, K.; Lee, R. T.; So, P. T. C. *J. Biomed. Opt.* **2007**, *12*, 014015.

(20) Choi, H.; Wadduwage, D. N.; Tu, T. Y.; Matsudaira, P.; So, P. T. C. *Cytometry Part A* **2015**, *87*, 49-60.

(21) Chieco, P.; Jonker, A.; Melchiorri, C.; Vanni, G.; Van Noorden, C. F. *Histochem J* **1994**, *26*, 1-19.

(22) Rodenacker, K.; Bengtsson, E. *Analytical Cellular Pathology* **2003**, *25*, 1-36.

(23) De Vos, W. H.; Van Neste, L.; Dieriks, B.; Joss, G. H.; Van Oostveldt, P. *Cytometry Part A* **2010**, *77A*, 64-75.

(24) Beverloo, H. B.; van Schadewijk, A.; van Gelderen-Boele, S.; Tanke, H. J. *Cytometry* **1990**, *11*, 784-792.

(25) Yuan, J.; Wang, G. *TrAC Trends in Analytical Chemistry* **2006**, *25*, 490-500.

(26) Rajapakse, H. E.; Gahlaut, N.; Mohandessi, S.; Yu, D.; Turner, J. R.; Miller, L. W. *Proceedings of the National Academy of Sciences* **2010**, *107*, 13582-13587.

(27) Lu, Y.; Jin, D.; Leif, R. C.; Deng, W.; Piper, J. A.; Yuan, J.; Duan, Y.; Huo, Y. *Cytometry Part A* **2011**, *79A*, 349-355.

(28) Li, L.-L.; Zhang, R.; Yin, L.; Zheng, K.; Qin, W.; Selvin, P. R.; Lu, Y. *Angewandte Chemie International Edition* **2012**, *51*, 6121-6125.

(29) Liu, Y.; Tu, D.; Zhu, H.; Ma, E.; Chen, X. *Nanoscale* **2013**, *5*, 1369-1384.

(30) Zhou, L.; Wang, R.; Yao, C.; Li, X.; Wang, C.; Zhang, X.; Xu, C.; Zeng, A.; Zhao, D.; Zhang, F. *Nat Commun* **2015**, *6*.

(31) Zhang, F.; Shi, Q.; Zhang, Y.; Shi, Y.; Ding, K.; Zhao, D.; Stucky, G. D. *Advanced Materials* **2011**, *23*, 3775-3779.

(32) Wang, F.; Deng, R.; Wang, J.; Wang, Q.; Han, Y.; Zhu, H.; Chen, X.; Liu, X. *Nat Mater* **2011**, *10*, 968-973.

(33) Lu, Y.; Lu, J.; Zhao, J.; Cusido, J.; Raymo, F. M.; Yuan, J.; Yang, S.; Leif, R. C.; Huo, Y.; Piper, J. A.; Paul Robinson, J.; Goldys, E. M.; Jin, D. *Nat Commun* **2014**, *5*.

(34) van de Rijke, F.; Zijlmans, H.; Li, S.; Vail, T.; Raap, A. K.; Niedbala, R. S.; Tanke, H. J. *Nat Biotech* **2001**, *19*, 273-276.

(35) Zhao, J.; Jin, D.; Schartner, E. P.; Lu, Y.; Liu, Y.; Zvyagin, A. V.; Zhang, L.; Dawes, J. M.; Xi, P.; Piper, J. A.; Goldys, E. M.; Monro, T. M. *Nat Nano* **2013**, *8*, 729-734.

(36) Zhang, L.; Zheng, X.; Deng, W.; Lu, Y.; Lechevallier, S.; Ye, Z.; Goldys, E. M.; Dawes, J. M.; Piper, J. A.; Yuan, J.; Verelst, M.; Jin, D. *Scientific Reports* **2014**, *4*, 6597.

(37) Lu, Y.; Zhao, J.; Zhang, R.; Liu, Y.; Liu, D.; Goldys, E. M.; Yang, X.; Xi, P.; Sunna, A.; Lu, J.; Shi, Y.; Leif, R. C.; Huo, Y.; Shen, J.; Piper, J. A.; Robinson, J. P.; Jin, D. *Nat Photon* **2014**, *8*, 32-36.

(38) Zhang, Y.; Zhang, L.; Deng, R.; Tian, J.; Zong, Y.; Jin, D.; Liu, X. *Journal of the American Chemical Society* **2014**, *136*, 4893-4896.

(39) Lu, Y.; Xi, P.; Piper, J. A.; Huo, Y.; Jin, D. *Sci. Rep.* **2012**, *2*, 837.

(40) Lu, J.; Martin, J.; Lu, Y.; Zhao, J.; Yuan, J.; Ostrowski, M.; Paulsen, I.; Piper, J. A.; Jin, D. *Analytical Chemistry* **2012**, *84*, 9674-9678.

(41) Li, Q.; Bai, L.; Xue, S.; Chen, L. *OPTICE* **2002**, *41*, 1289-1294.

(42) Leif, R. C.; Yang, S.; Jin, D.; Piper, J.; Vallarino, L. M.; Williams, J. W.; Zucker, R. M. *J. Biomed. Opt.* **2009**, *14*, 024022-024022-7.

(43) Lu, J.; Chen, Y.; Liu, D.; Ren, W.; Lu, Y.; Shi, Y.; Piper, J. A.; Paulsen, I. T.; Jin, D. *Analytical Chemistry* **2015**.

(44) Bravo-Zanoguera, M.; v. Massenbach, B.; Kellner, A. L.; Price, J. H. *Review of Scientific Instruments* **1998**, *69*, 3966-3977.

(45) Braeckmans, K.; De Smedt, S. C.; Leblans, M.; Pauwels, R.; Demeester, J. *Nat Rev Drug Discov* **2002**, *1*, 447-456.

(46) Wilson, R.; Cossins, A. R.; Spiller, D. G. *Angewandte Chemie International Edition* **2006**, *45*, 6104-6117.

(47) Fulton, R. J.; McDade, R. L.; Smith, P. L.; Kienker, L. J.; Kettman, J. R. *Clinical Chemistry* **1997**, *43*, 1749-1756.

(48) Han, M.; Gao, X.; Su, J. Z.; Nie, S. *Nat Biotech* **2001**, *19*, 631-635.

(49) Li, Y.; Cu, Y. T. H.; Luo, D. *Nat Biotech* **2005**, *23*, 885-889.

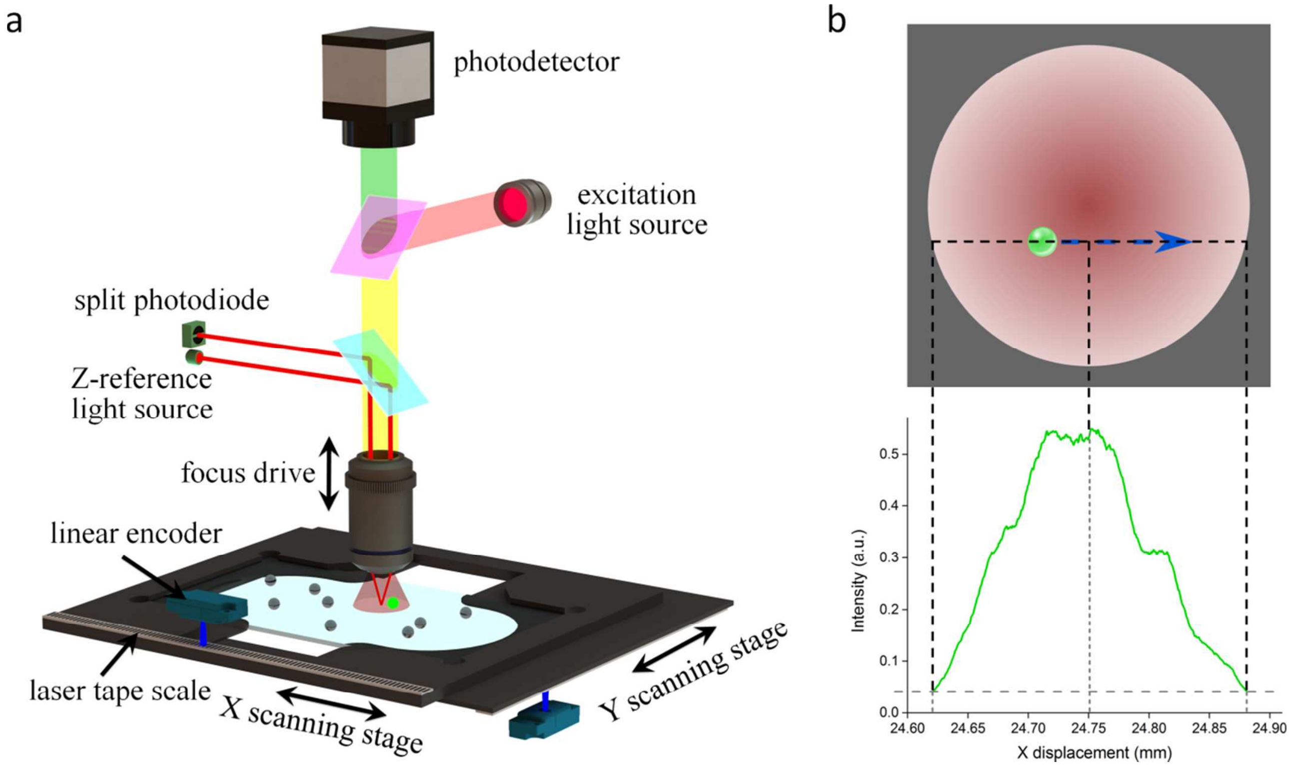

Figure 1. (a) Schematic illustrating the concept of R-OSAM, which exploits linear encoders and autofocusing to pinpoint targets during rapid scanning of the sample slide. For each of the scan direction (X and Y), a laser tape scale is attached to the stage, and a linear encoder is mounted (fixed to the microscope frame) above the scale to read the displacement when the stage moves. The output is correlated to the luminescence signal recorded by the photodetector to determine the precise location of the target along the scan direction. To enable the autofocus function of the sample slide, a Z-reference light source delivers its beam in the margin of the optical path, so that any change in the focal length will lead to the shift of the reflected beam. This is detected by a split photodiode, which feedback controls the focus drive to maintain the focal length. (b) The sunrise-sunset luminescence signal profile with respect to the scan displacement of one typical target passing across the field of view (FOV), from which the location of the target along the scan direction is obtained.

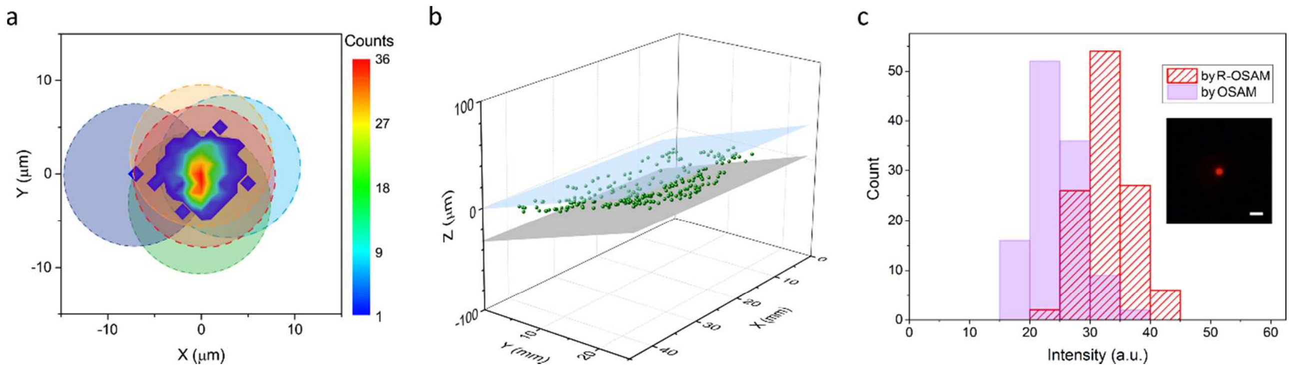

Figure 2. (a) A heat plot summarising the locations of the UCNP-impregnated calibration beads obtained by the R-OSAM with respect to the centre of the FOV for a typical sample slide, with the shadowed circles indicating the size of the beads (15 μm). (b) The spatial distribution of UCNP-impregnated beads spread between a microscopic slide and a cover slip, measured by the R-OSAM. The standard deviations for the Z-coordinate of the bead and for the distance from each bead to the substrate plane are 16.2 μm and 6.7 μm respectively, suggesting that the tilt of the slide is usually the major cause of the variance in focus. (c) Comparison of luminescence intensity profiles for 5 μm Eu-calibration beads on the same sample slide, measured by the R-OSAM (red bars) and the OSAM with both encoders and autofocus disabled (purple bars). Exposure time: 100 ms. Scale bar: 15 μm.

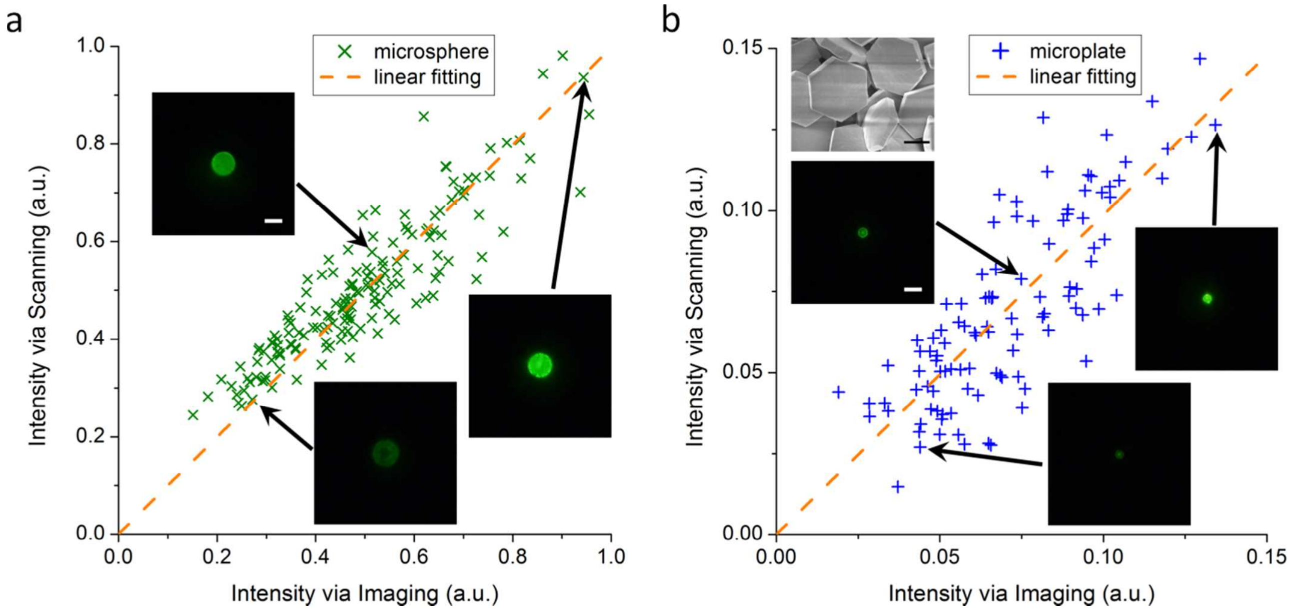

Figure 3. Correlation between the luminescence intensity captured by the R-OSAM and that measured from the image taken after target retrieval, for (a) 15 μm UCNP-impregnated microspheres, and (b) upconversion microplates (Scanning Electron Microscopy image on the top left corner), over a large dynamic range. Each of the luminescence images show an individual microsphere or microplate that generates the data point, with exposure times of 50 ms for the microspheres and 150 ms for the microplates, respectively. Scale bars represent 15 μm in the luminescence image and 2 μm in the SEM image.

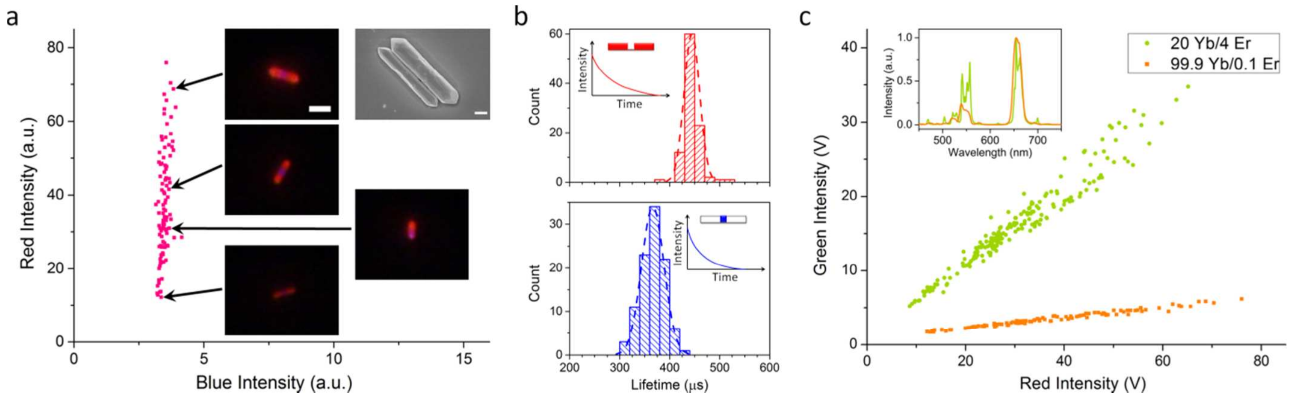

Figure 4. (a) A scatter plot showing the luminescence intensities measured by the R-OSAM in the red (ends) and the blue channels (middle) from individual upconversion microrods (SEM image on the top right corner), alongside representative luminescence images taken after target retrieval. Exposure time is 150 ms. Scale bars represent 5 μm in the luminescence image and 1 μm in the SEM image. (b) Histograms of the luminescence lifetimes for the ends (red channel) and the middle (blue channel) of the microrods. (c) The intensity ratios of green to red luminescence with respect to the Yb/Er co-doping concentrations. The inset shows normalised emission spectra.

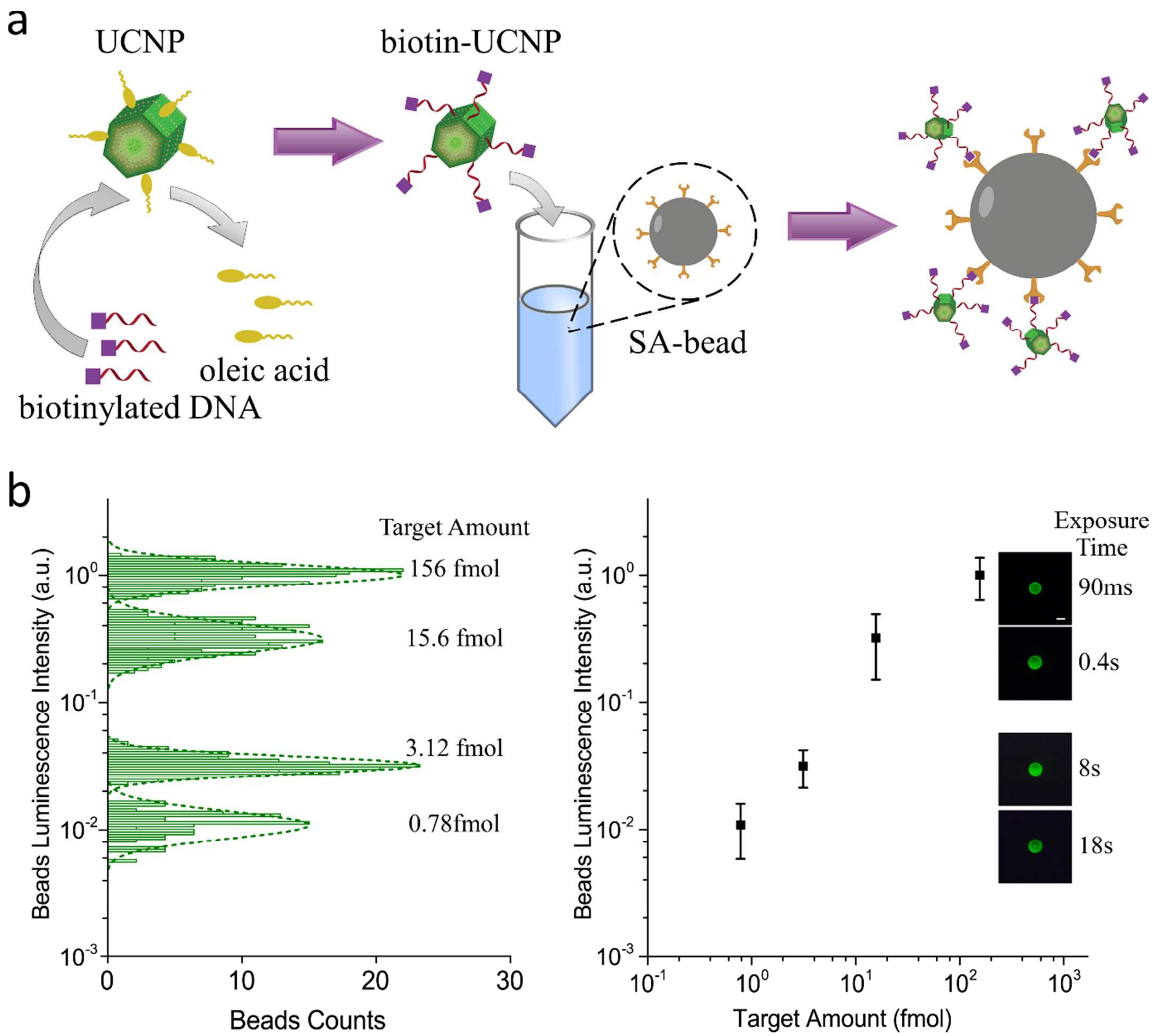

Figure 5. (a) The scheme of the demonstration assay using biotinylated-DNA functionalised UCNPs as the target and SA conjugated polystyrene beads as the substrate. (b) The relation between the amount of the biotin-UCNPs and the luminescence intensity of individual beads, concluded statistically from the intensity histograms of the beads populations. The error bars represent twice the standard deviation (95% confidence). The inset images show typical beads from each population, captured with different exposure time. Scale bar 10 µm.